

# A NOVEL AND EFFICIENT FINITE ELEMENT SOFTWARE FOR HEAT TRANSFER: FEHEAT

A. Serdar Selamet, Boğaziçi University, Turkey

B. Murat Uzun, Boğaziçi University, Turkey

## ABSTRACT

Fire poses a great threat to steel structures. Since fire experiments are expensive and furnaces are usually limited both in number and in size, finite element (FE) analysis programs are utilized to conduct both heat transfer and structural analyses. In order to accurately model structural fire problems, it is essential to estimate the material temperatures correctly. In this study, a novel FE program in MATLAB, a widely available commercial numerical software, is developed. FE code solves the parabolic partial differential equation of transient heat transfer in two dimensions with nonlinear convective and radiative boundary conditions. The program uses backward, forward or central difference for progression in time and full Newton-Raphson method for convergence between increments. The program is specially designed for cross sections of the wide flange beams. The original contribution of FEHEAT program is the inclusion of view (configuration) factors to the nonlinear solution algorithm. FEHEAT program is vigorously validated with established FE software Abaqus. Several case studies are conducted for various types of steel wide-flange cross sections. The results show that the inclusion of radiation heat exchange between bottom flange and top flange via the view factors significantly increases the temperature in the regions away from the fire boundary. The surface heat exchange by radiation causes as much as 50% decrease in the thermal gradient for various cross sections, which is a crucial advantage especially for one-side heated perimeter columns.

## NOMENCLATURE

M = Mass matrix

T = Temperature field vector

K = Global conduction/stiffness matrix

K<sub>e</sub> = Element conduction/stiffness matrix

$\dot{T}$  = Temperature derivative field vector

$\widehat{T}$  = Temperature field predictor

T<sub>o</sub> = Initial temperature field

N = Shape function vector for the four nodes of each element

F = Heat flux vector

R = Unbalanced heat vector

J = Jacobian matrix

J<sub>r</sub> = Nonlinear contribution (radiation) of the heat flux vector

v<sub>o</sub> = Temperature velocity vector

$\alpha$  = Trapezoid rule coefficient

F<sub>ij</sub> = View factor between element i and j

$\vec{n}$  = Surface normal vector

$\vec{s}_{ij}$  = Distance vector between element i and j

dA<sub>i,j</sub> = Differential area element

$\vec{s}_{ij}$  = Distance vector

dF<sub>p,i</sub> = Viewfactor coefficient from one point on a differential strip

T<sub>y</sub> = Thermal gradient

## 1. INTRODUCTION

The correct estimation of the temperatures in structural member cross sections is crucial to calculate fire induced forces and moments and ultimately to evaluate the fire performance of the structural system. With increasing computational power, and mathematical know-how, the finite element (FE) analysis software are utilized to conduct both heat transfer and structural analyses since fire experiments are expensive and furnaces are usually limited both in number and in size.

In this study, a finite element code FEHEAT with a Graphical User Interface (GUI) is developed using MATLAB. GUI is specifically designed for structural fire engineers and it is limited to wide-flange beam sections with or without fire protection. In wide-flange sections, the top and bottom flanges as well as the web constitute an enclosure and hence in addition to convective and radiative heat transfer on the fire boundary, the surfaces in the enclosure exchange heat by radiation. Such problem requires the calculation of geometric surface-to-surface radiation view factors. The view factors for three-dimensional body of any geometry can be calculated by either area or line integration algorithms [1]. The calculation of such integrals is

tedious and numerical integration techniques are generally employed [2].

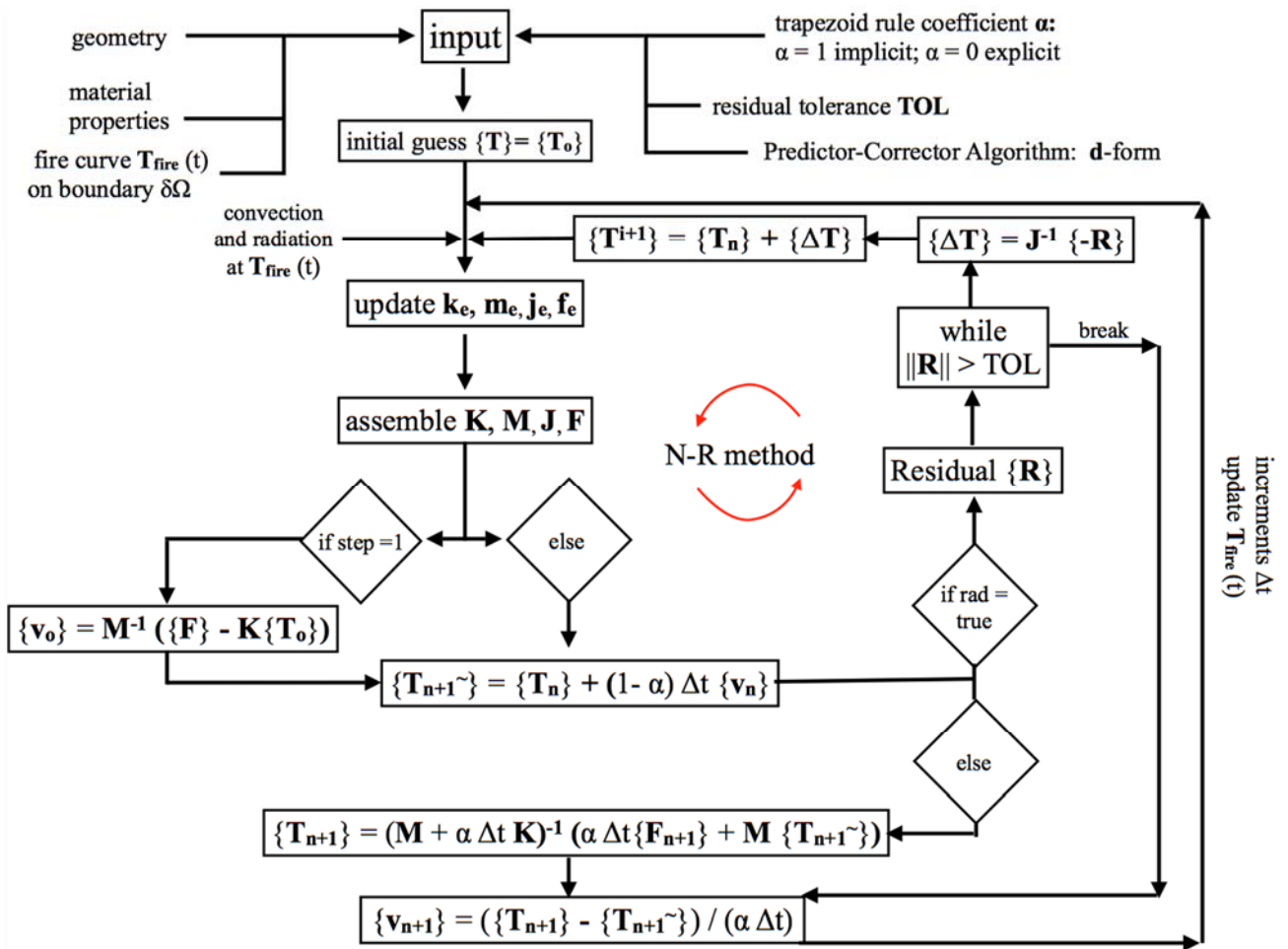
Using this code, the objective is to run fast and reliable parametric studies with various wide-flange beam sections and investigate the effect of section dimensions and surface heat exchange by radiation on the thermal gradient, which is an important parameter to calculate the fire performance of perimeter columns. Observations and numerical analyses suggest that the enclosure radiation does not affect the temperature field if the wide-flange sections are subjected to fire on three sides (i.e. all surfaces except the top surface) [3]. In the case of perimeter columns, the top surface of the flange is considered as the only fire boundary, which will create a large thermal gradient in the

cross section. If the effect of the surface heat exchange by radiation is taken into account, the thermal gradient will be reduced [4].

## 2. FEHEAT FINITE ELEMENT CODE

FEHEAT solves the parabolic partial differential equation of nonlinear transient heat transfer in two dimensions with convective and radiative boundary conditions. The user can also specify a pre-described temperature or direct heat flux on the fire boundary. The program uses backward, forward or central difference for progression in time and full Newton-Raphson method for convergence between increments. The full details of the step-by-step procedures are given in Table 1.

**Table 1: Flowchart of the FEHEAT algorithm for linear and non-linear heat transfer analysis**



The semi-discrete parabolic heat equation is written with an initial condition (temperature) as in Eq. 2.1 and 2.2. The heat equation is semi-discrete because the finite element method is used to solve the

problem for the entire domain at a specific time, whereas stepping to the next time step is achieved by using the finite difference method. The most commonly used time stepping algorithm for solving

the parabolic heat equation is the generalized trapezoidal family of methods (see Table 2).

$$[M]\{\dot{T}\} + [K]\{T\} = \{F\} \quad (2.1)$$

$$\{T(0)\} = \{T_0\} \quad (2.2)$$

The time stepping algorithm starts with the initial temperature field  $\{T_0\}$ . As shown in Eq. 2.3, the solution propagates in time using the predictor-corrector method using the coefficient  $\alpha$  (scalar). The members of the generalized trapezoidal family are identified in Table 2.

$$\begin{aligned} \{v_{n+1}\} + [K]\{T_{n+1}\} &= \{F_{n+1}\} \\ \{T_{n+1}\} &= \{T_n\} + \Delta t \{v_{n+\alpha}\} \\ \{v_{n+\alpha}\} &= (1 - \alpha)\{v_n\} + \alpha \{v_{n+1}\} \end{aligned} \quad (2.3)$$

**Table 2: Trapezoidal families for the semi-discrete time stepping algorithm**

$\alpha$	name
0	Forward Euler
$\frac{1}{2}$	Crank-Nicolson
1	Backward Euler

Once the initial temperature field  $\{T_0\}$  is known, the initial temperature velocity vector  $\{v_0\}$  is evaluated at  $t = 0$  as in Eq. 2.4. Next, the predictor value  $\{\tilde{T}_{n+1}\}$  is found using Eq. 2.5. There are two implementations to predict the next step: v-form and d-form. The v-form implementation uses the velocity in order to predict the temperature and d-form calculates the temperature field in order to get the velocity field.

Both implementations have identical results, but d-form is computationally advantageous when the mass matrix  $[M]$  is diagonal.

$$[M]\{v_0\} = \{F_0\} - [K]\{T_0\} \quad (2.4)$$

$$\{\tilde{T}_{n+1}\} = \{T_n\} + (1 - \alpha) \Delta t \{v_n\} \quad (2.5)$$

*v-form:*

The velocity vector of the next step  $\{v_{n+1}\}$  is calculated by inverting the coefficient matrix as in Eq. 2.6. Finally, the recursion relation is ended by estimating the temperature field  $\{T_{n+1}\}$  of the next step (Eq. 2.7) and the iteration is continued to further steps.

$$([M] + \alpha \Delta t [K]) \{v_{n+1}\} = \{F_{n+1}\} [K] \{\tilde{T}_{n+1}\} \quad (2.6)$$

$$\{T_{n+1}\} = \{T_n\} + \alpha \Delta t \{v_{n+1}\} \quad (2.7)$$

*d-form:*

For this implementation, the temperature vector of the next step  $\{d_{n+1}\}$  is first calculated by inverting the coefficient matrix as in Eq. 2.8. Finally, the recursion relation is ended by estimating the velocity field  $\{v_{n+1}\}$  of the next step (Eq. 2.9) and the iteration is continued to further steps.

$$\frac{1}{\alpha \Delta t} ([M] + \alpha \Delta t [K]) \{T_{n+1}\} = \{F_{n+1}\} + \frac{1}{\alpha \Delta t} [M] \{\tilde{T}_{n+1}\} \quad (2.8)$$

$$\{v_{n+1}\} = \frac{\{T_n\} - \{\tilde{T}_{n+1}\}}{\alpha \Delta t} \quad (2.9)$$

## 2.1 NONLINEAR SOLUTION ALGORITHM

The heat transfer problem is non-linear due to the radiation boundary conditions at the fire surface and surface heat exchange by radiation in the enclosure. For the nonlinear problem, a full Newton-Raphson (NR) iteration scheme is used. N-R requires to assemble the tangent stiffness matrix at each iteration  $i$  of each time increment  $n$ . The tangent stiffness matrix is also called the Jacobian matrix  $[J]$  in the structural engineering practice. Here, only a brief explanation of NR methodology is provided and a more detailed explanation can be found by [5].

First, the unbalanced heat vector  $\{R\}$  is formed from Eq. 2.8 (d-form) as defined in Eq. 2.10 (see Table 1).  $\{R\}$  is estimated using the temperature field from the previous step  $\{T\}$  and the temperature field predictor  $\{\tilde{T}\}$ . The terms of the contribution to the Jacobian matrix  $J_{ij}$  are the derivatives of the unbalanced heat load vector as shown in Eq. 2.11.

$$\{R\} = \frac{1}{\alpha \Delta t} ([M] + \alpha \Delta t [K]) \{T\} - \frac{1}{\alpha \Delta t} [M] \{\tilde{T}\} - \{F\} \quad (2.10)$$

$$J_{ij} = \frac{\partial R_i}{\partial T_j} = 4 \int_{S4} \sigma \epsilon T^3 \frac{\partial T}{\partial T_j} N_i d\Gamma \quad (2.11)$$

Equation 2.12 is the vectorized notation of Equation 2.11 and it defines the contribution of the nonlinear heat flux term  $[J_r]$  to the global conduction matrix of the solid body. Equation 2.13 is the global Jacobian matrix  $[J]$ .

$$[J_r] = 4 \int_{S^4} \sigma \epsilon T^3 \{N\} |N| d\Gamma \quad (2.12)$$

$$[J] = \left( [K] + \frac{1}{\alpha \Delta t} [M] \right) + [J_r] \quad (2.13)$$

Once the global Jacobian matrix is assembled, NR algorithm is performed as below at increment  $n$  until a specified tolerance value (TOL in Table 1) is reached:

$$\begin{aligned} \{\Delta T_{n+1}^{i+1}\} &= [J_{n+1}^i]^{-1} \{-R_{n+1}^i\} \\ \{T_{n+1}^{i+1}\} &= \{T_{n+1}^i\} + \{\Delta T_{n+1}^{i+1}\} \end{aligned} \quad (2.14)$$

### 3. VIEW FACTOR CALCULATION

In the absence of an absorbing medium, radiative heat exchange between surfaces depends on the optical view of each surface to the others as seen in Fig. 1. The view factor estimation for surfaces involves rigorous methods and the different methods can be classified by the way in which the integration is carried out. Several methods can be used such as contour integration, area integration, crossed-strings method, unit sphere method or Monte-Carlo method. Among these methods, the area integration method for finite elements is chosen for its efficient algorithm and easy implementation to the finite element code.

The view factor equation is constructed by solving the general radiation exchange equation of arbitrary inclined finite surfaces. If the surfaces are diffuse and have a spatially constant emissive power, the fraction of radiant energy leaving surface  $i$  that is intercepted by surface  $j$  is:

$$F_{ij} = \frac{1}{A_i} \iint \frac{\cos \theta_i \cos \theta_j}{\pi S^2} dA_j dA_i \quad (3.1)$$

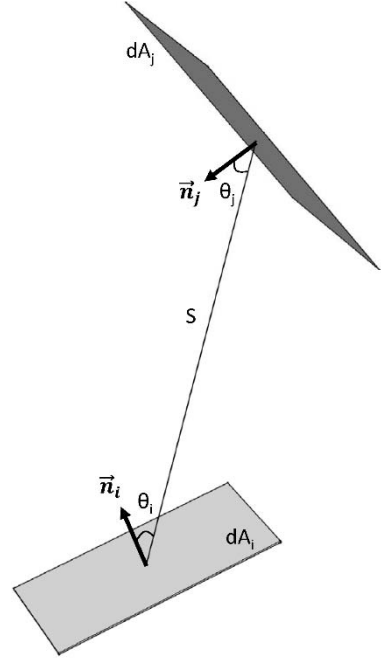


Fig. 1. The optical view of finite surface  $dA_i$  and surface  $dA_j$ .

#### 3.1 FROM 3D TO 2D

Eq. 3.1 calculates the view factor coefficients for surface areas in three-dimensions. However, for a two-dimensional heat transfer analysis, the finite surfaces become finite strips (lines). Eq. 3.1 is therefore modified for reduced space dimensions. In the next steps, an equation for the view factor coefficient of finite strips with infinitely long width is derived.

As illustrated in Fig. 2, let  $\vec{s}_{ij}$  be the distance vector from a point on Surface  $dA_i$  to a point on Surface  $A_j$  as in Eq. 3.2:

$$\vec{s}_{ij} = -\vec{s}_{ji} = \vec{r}_j - \vec{r}_i = (x_j - x_i)\vec{i} + (y_j - y_i)\vec{j} + (z_j - z_i)\vec{k} \quad (3.2)$$

The local surface normal (unit) vector for each finite surface area can be written as:

$$\vec{n} = \cos \theta_x \vec{i} + \cos \theta_y \vec{j} + \cos \theta_z \vec{k} \quad (3.3)$$

where  $\cos \theta_x, \cos \theta_y, \cos \theta_z$  are direction cosines for the unit vector  $\vec{n}$ .

The angles between the surface normal and the distance vector  $\vec{s}$  are shown in Eq. 3.4:

$$\cos\theta_i = \frac{\vec{n}_i \cdot \vec{s}_{ij}}{S} = \frac{1}{S} [(x_j - x_i) \cos\theta_{x,i} + (y_j - y_i) \cos\theta_{y,i} + (z_j - z_i) \cos\theta_{z,i}]$$

$$\cos\theta_j = \frac{\vec{n}_j \cdot \vec{s}_{ji}}{S} = \frac{1}{S} [(x_i - x_j) \cos\theta_{x,j} + (y_i - y_j) \cos\theta_{y,j} + (z_i - z_j) \cos\theta_{z,j}]$$

(3.4)

where  $S = \sqrt{|\vec{s}_{ji}|^2}$  is the distance length from the center of surface  $i$  to the center of surface  $j$ .

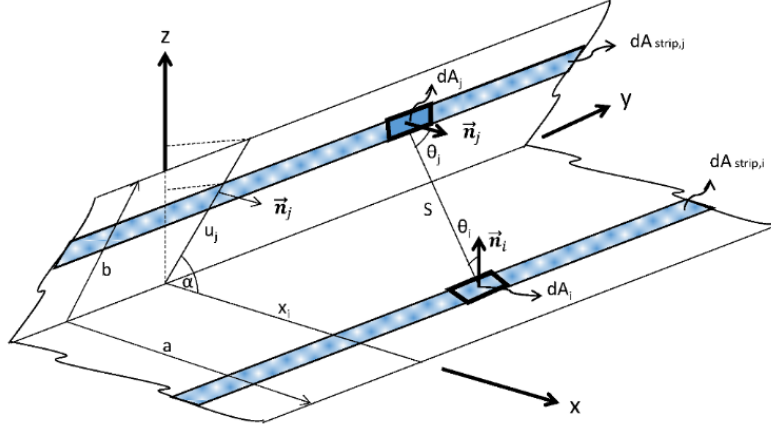


Fig. 2. The calculation of the viewfactor coefficient of finite surfaces (in 3D) at arbitrarily angle  $\alpha$  with infinite dimension in y-axis.

As seen in Fig. 2,  $z_i = 0$ ;  $x_j = u_j \cos(\alpha)$  and  $z_j = u_j \sin(\alpha)$  leads to

$$S^2 = S_o^2 + (y_1 - y_2)^2 \quad (3.5)$$

where  $S_o$  is the projection of  $S$  in the x-z-plane.

The surface normal  $\vec{n}_i$  and  $\vec{n}_j$  are readily determined as shown in Eq. 3.6:

$$\begin{aligned} \vec{n}_i &= \vec{k} \\ \vec{n}_j &= \vec{i} \sin\alpha - \vec{k} \cos\alpha \end{aligned} \quad (3.6)$$

For this problem, Eq. 3.4 reduces to Eq. 3.7:

$$\begin{aligned} \cos\theta_i &= u_j \sin\alpha / S \\ \cos\theta_j &= x_i \sin\alpha / S \end{aligned} \quad (3.7)$$

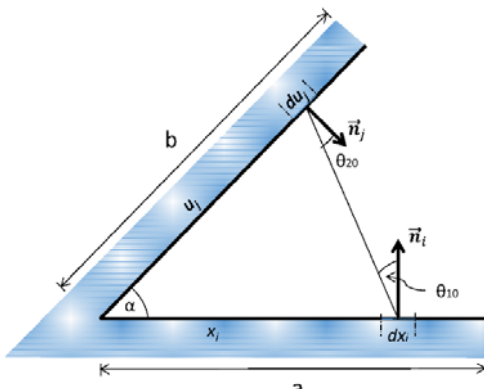


Fig. 3. The viewfactor calculation of the finite strips in 2D.

The viewfactor coefficient from *one point* on a differential strip ( $dF_{p,i}$ ) to a finite strip ( $strip_j$ ) is therefore:

$$\begin{aligned} dF_{p,i-strip,j} &= \int \frac{\cos\theta_i \cos\theta_j}{\pi S^2} dA_j \\ &= \frac{du_j}{\pi} \int_{-\infty}^{\infty} \frac{x_i u_j \sin^2\alpha dy_j}{[S_o^2 + (y_i - y_j)^2]^2} \end{aligned} \quad (3.8)$$

If  $\theta_{10}$  and  $\theta_{20}$  are assumed to be the projections of  $\theta_i$  and  $\theta_j$ , the final equation is found. Eq. 3.9 gives the view factor coefficient of one point  $p$  in finite strip  $i$  to a finite strip  $du_j$ .

$$dF_{p,i-strip,j} = \frac{1}{2} \cos\theta_{i0} \cos\theta_{j0} \frac{du_j}{S_o} \quad (3.9)$$

#### 4. IMPLEMENTATION OF VIEWFACTOR CALCULATION

The viewfactor coefficient of each element in an enclosure of the wide-flange section is calculated at the beginning of FEHEAT code. Each finite element is divided to sub-elements ( $m$  sub-elements for element  $i$  and  $n$  sub-elements for element  $j$ ). In order to calculate the viewfactor coefficient  $F_{ij}$  of the finite element  $i$  to finite element  $j$ , the procedure

illustrated in Fig. 4 is used. Eq. 3.9 is integrated by Riemann Summation of each sub-element.

$$F_{ij} = \frac{1}{m} \sum_m \sum_n \frac{1}{2} \cos \theta_{io,m} \cos \theta_{jo,n} \frac{du_{m-n}}{S_{o,m-n}} \quad (4.1)$$

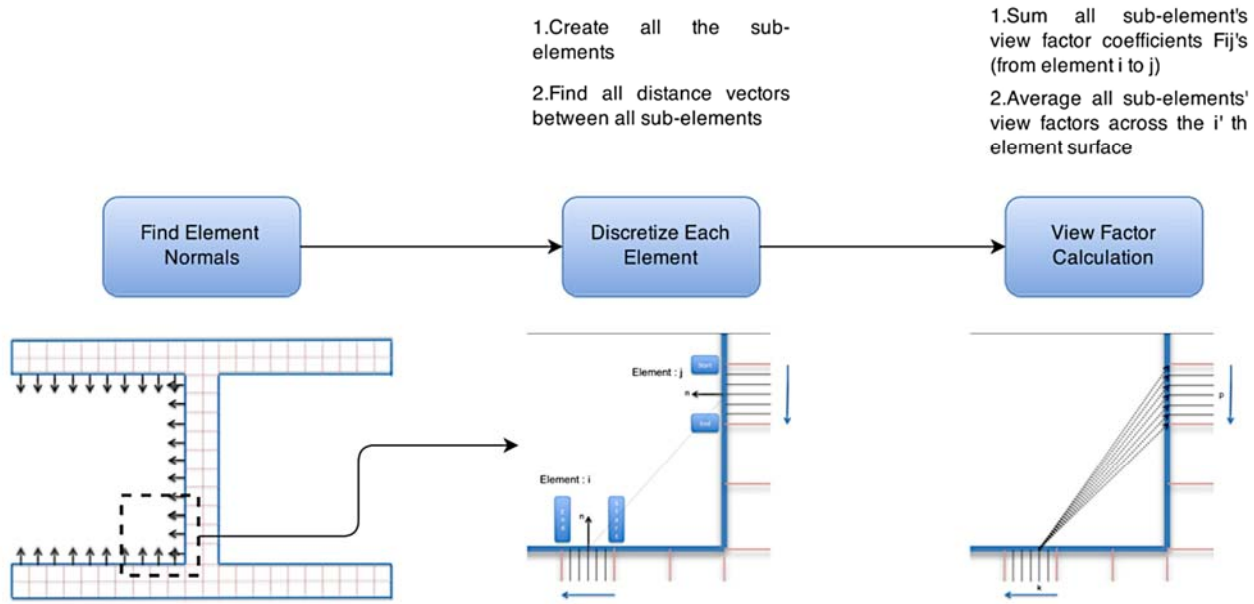


Fig. 4 The implementation in FEHEAT to find the viewfactor coefficients  $F_{ij}$  for each finite element in an enclosure.

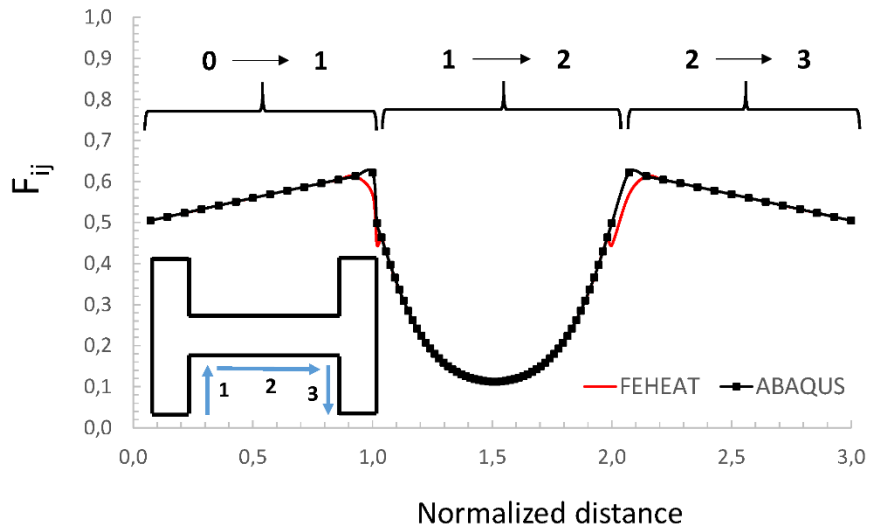


Fig. 5. The viewfactor  $F_{ij}$  validation for wide-flange section with Abaqus

The results are validated by Abaqus, a commercially available finite element software [6]. The viewfactor coefficients of the wide-flange section enclosure in FEHEAT match very closely to the coefficients in Abaqus as seen in Fig. 5. Here, only 6 sub-elements are used and as the number of sub-elements increases, the results converge.

## 5. PARAMETRIC STUDY AND RESULTS

Once the viewfactor algorithm is validated, a parametric study is conducted to see the effect of geometric dimensions of the wide-flange steel sections on the surface heat exchange by radiation. Since the viewfactor coefficient is a geometric property, the geometric properties of the wide-flange beams ( $d$ ,  $b_f$ ,  $t_f$ ,  $t_w$ ) might have a significant effect on the heat flux between the heated region and the cooler region.

In order to conduct a parametric study with realistic dimensions, the steel profiles from the American Institute of Steel Construction (AISC) are used [7]. Table 3 summarizes the statistics of the characteristic dimensions of over 270 wide-flange sections.

Over 30 wide-flange sections are selected. The range of the depth  $d$  varied from 100mm to 1000mm and the range of the flange width  $b_f$  is from 100mm to 600mm. The flange and web thickness ( $t_f$  and  $t_w$ ) are kept constant to isolate the effect of the depth and flange width, which essentially constitute the enclosure dimensions.

Columns are the most critical structural members for the global stability of the buildings. During fire, the perimeter columns are likely to be subjected to fire on one-side if the walls are good insulators such as brick or gypsum board. Even if the columns are

fire-protected, the one-sided heating will create large thermal gradient in addition to compression with thermal expansion. The thermal gradient will create additional moment due to the shift of the stiffness centroid of the wide-flange section [8, 9]. Hence, the effect of the thermal gradient  $T_y$  is investigated with the consideration of the surface heat exchange by radiation.

The perimeter columns heated only on one side are taken as a case study as illustrated in Fig. 6. The unexposed (to fire) boundaries exchange heat by radiation when the surface-to-surface radiation (via view factors) is enabled. Otherwise, the unexposed boundaries are adiabatic. The columns are subjected to ISO-834 fire curve for 90 minutes. In order to observe the worst-case scenario, no fire protection is applied to the columns.

**Table 3. Mean, maximum and minimum values of wide-flange section dimensions in AISC. All dimensions are in mm.**

section dimensions	max	min	mean	section dimension ratios	max	min	mean
$d$	1120	106	573	$d / b_f$	3.39	0.95	2.01
$b_f$	455	100	288	$d / t_f$	52.80	4.55	22.21
$t_f$	125	5	32	$d / t_w$	62.94	7.29	35.55
$t_w$	78	4	19	$b_f / t_f$	23.03	3.64	11.19
				$b_f / t_w$	32.86	5.83	17.94
				$t_f / t_w$	1.90	1.10	1.64

The heat transfer analysis is conducted for each wide-flange section with and without the surface heat exchange by radiation. The thermal gradient  $T_y$  is simply calculated by subtracting the bottom flange average temperature from the top flange average temperature and dividing the result by the depth of the section for the duration of the fire.

Fig. 7 shows the time when the maximum thermal gradient occurs. As expected, the thermal gradient is generally largest at the end of the fire curve (90 min) without the surface heat exchange. However, the time for maximum thermal gradient is scattered from 40 to 90 min if the surface heat exchange is allowed.

The results are shown in Fig. 8. Each point on the surfaces represents  $T_{y,max}$  for each parametric study. The surfaces are created by cubic interpolation of these points. The  $T_{y,max}$  is a function of the depth ( $d$ ) and the flange width ( $b_f$ ). The top surface represents  $T_{y,max}$  without the consideration of surface heat exchange and the bottom surface represents  $T_{y,max}$  with the consideration of surface heat exchange.

Fig. 8 suggests that the heat exchange between the bottom flange, top flange and the web in enclosure reduces the thermal gradient significantly for the entire range of the wide-flange sections. The percent decrease of  $T_{y,max}$  could be as much as 50%. The  $T_{y,max}$  rapidly increases for  $d/b_f < 1.0$ . When the depth is large, increasing the flange width does not affect the  $T_{y,max}$ . Overall, the  $T_{y,max}$  seems to be

correlated more with the depth of the section than the flange width.

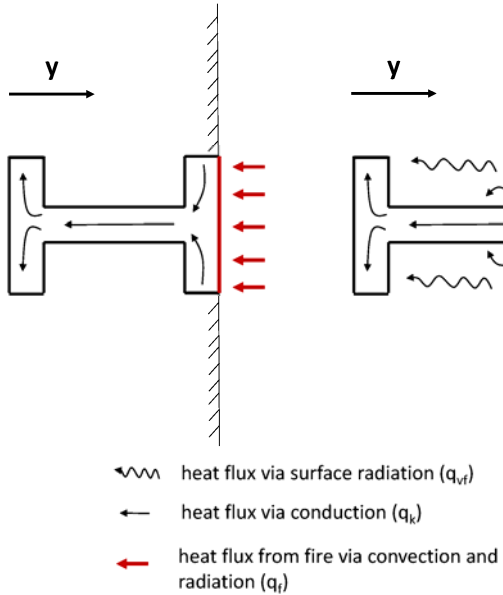


Fig. 6 The effect of surface heat exchange by radiation in one-side heated perimeter columns.

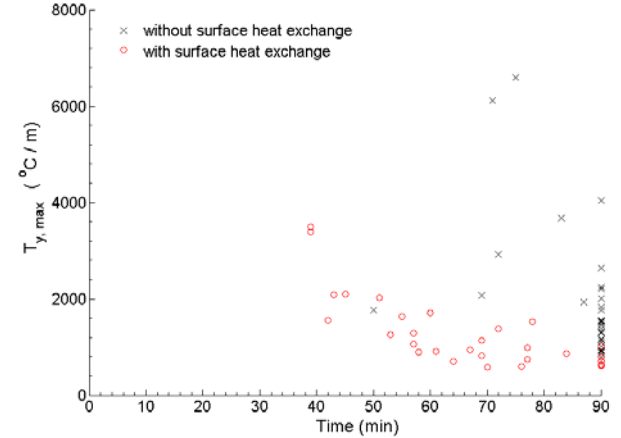


Fig. 7. The time when the maximum thermal gradient  $T_{y,max}$  is reached with and without the surface heat exchange by radiation in the enclosure.

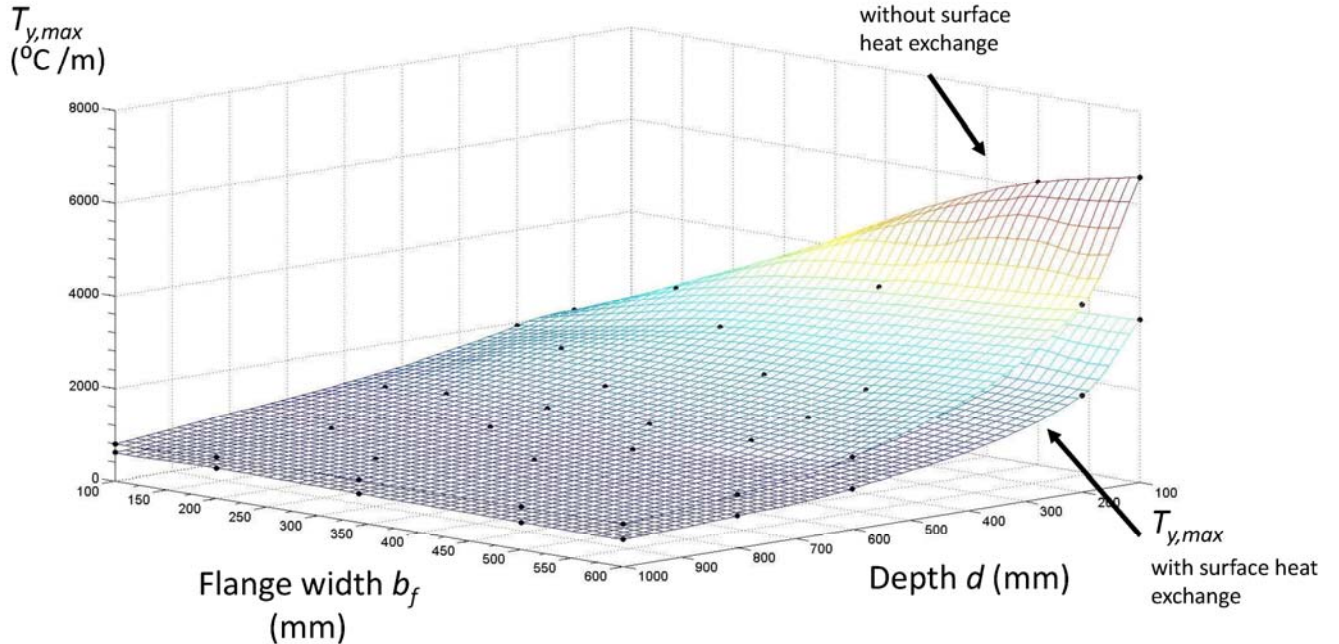


Fig. 8. The maximum thermal gradient  $T_{y,max}$  surface as a function of the depth ( $d$ ) and the flange width ( $b_f$ ) with and without the surface heat exchange by radiation in the enclosure.

## 6. CONCLUSIONS

This paper presents an on-going research on the development of a novel finite element code FEHEAT, which is specifically designed for structural fire engineers. FEHEAT solves the parabolic partial differential equation of nonlinear

transient heat transfer in two dimensions with convective and radiative fire boundary conditions. FEHEAT has also the capability to calculate the viewfactor coefficients (in 2D) in a wide-flange section enclosure to take account of the surface heat exchange by radiation. The effect of the heat exchange is confirmed via the perimeter columns

heated on one-side with a standard fire curve. The analyses show that the most significant effect of the surface heat exchange is on the thermal gradient in the columns. Depending on the geometric dimensions of the enclosure ( $d$  and  $b_f$ ), the reduction in the maximum thermal gradient in the cross section could be as much as 50%. Such reduction confirms that the additional moment on the column induced by the thermal gradient is significantly reduced. Therefore, the estimation of the moments due to section thermal gradient with adiabatic surfaces in the enclosure is a very conservative approach.

[5] Huebner, K. H., Dewhirst, D. L., Smith, D. E., & Byrom, T. G. (2008). ‘*The finite element method for engineers*’, John Wiley & Sons.

[6] DS-Simulia. (2012). ‘*ABAQUS/Standard User’s Manual Version 6.12*’, Providence, RI.

[7] American Institute of Steel Construction (2005). *Steel Construction Manual*, Chicago IL.

[8] Selamet S., Garlock M., (2013). ‘Fire resistance of steel shear connections’, *Fire Safety Journal*, 68: 52-60.

[9] Selamet S., Garlock M., (2013). ‘Plate buckling strength of steel wide-flange sections at elevated temperatures’, *J Struct Eng*, 139(11): 1853-1865.

## ACKNOWLEDGEMENTS

The authors acknowledge the Marie Curie International Incoming Fellowship (FP7-PEOPLE-2012-IIF) “Fire Resistance of Connections in a Composite Floor System”: CONFIRE 328993, Bogazici University Scientific Research Project BAP: 7122P and 3001-TUBITAK Project: 114M791, which provided the funding for this study.

## REFERENCES

- [1] Shapiro, A. B. (1985). ‘Computer implementation, accuracy, and timing of radiation view factor algorithms’, *Journal of heat transfer*, 107(3), 730-732.
- [2] Emery, A. F., Johansson, O., Lobo, M., & Abrous, A. (1991). ‘A comparative study of methods for computing the diffuse radiation viewfactors for complex structures’, *Journal of heat transfer*, 113(2), 413-422.
- [3] Ghojel, J. I., & Wong, M. B. (2005). ‘Heat transfer model for unprotected steel members in a standard compartment fire with participating medium’, *Journal of Constructional Steel Research*, 61(6), 825-833.
- [4] Virdi, K. S., & Wickström, U (2013). ‘Influence of shadow effect on the strength of steel beams exposed to fire’, In *20th International Conference on Computer Methods in Mechanics*.